



Tuning the Bandgap Character of Quantum-Confined Si–Sn Alloyed Nanocrystals

Bürkle, M., Lozac'h, M., McDonald, C., Macias-Montero, M., Alessi, B., Mariotti, D., & Švrček, V. (2020). Tuning the Bandgap Character of Quantum-Confined Si–Sn Alloyed Nanocrystals. *Advanced Functional Materials*, 30(22), 1907210. [1907210]. <https://doi.org/10.1002/adfm.201907210>

[Link to publication record in Ulster University Research Portal](#)

Published in:
Advanced Functional Materials

Publication Status:
Published (in print/issue): 26/05/2020

DOI:
[10.1002/adfm.201907210](https://doi.org/10.1002/adfm.201907210)

Document Version
Publisher's PDF, also known as Version of record

General rights
Copyright for the publications made accessible via Ulster University's Research Portal is retained by the author(s) and / or other copyright owners and it is a condition of accessing these publications that users recognise and abide by the legal requirements associated with these rights.

Take down policy
The Research Portal is Ulster University's institutional repository that provides access to Ulster's research outputs. Every effort has been made to ensure that content in the Research Portal does not infringe any person's rights, or applicable UK laws. If you discover content in the Research Portal that you believe breaches copyright or violates any law, please contact pure-support@ulster.ac.uk.

Tuning the Bandgap Character of Quantum-Confined Si–Sn Alloyed Nanocrystals

Marius Bürkle,* Mickaël Lozac'h, Calum McDonald, Manuel Macias-Montero, Bruno Alessi, Davide Mariotti, and Vladimir Švrček

Nanocrystals in the regime between molecules and bulk give rise to unique electronic properties. Here, a thorough study focusing on quantum-confined nanocrystals (NCs) is provided. At the level of density functional theory an approximate (quasi) band structure which addresses both the molecular and bulk aspects of finite-sized NCs is calculated. In particular, how band-like features emerge with increasing particle diameter is shown. The quasiband structure is used to discuss technological-relevant direct bandgap NCs. It is found that ultrasmall Sn NCs have a direct bandgap in their at-nanoscale-stable α -phase and for high enough Sn concentration ($\approx 41\%$) alloyed Si–Sn NCs transition from indirect to direct bandgap semiconductors. The calculations strongly support recent experiments suggesting a direct bandgap for these systems. For a quantitative comparison many-body GW + Bethe–Salpeter equation (BSE) calculations are performed. The predicted optical gaps are close to the experimental data and the calculated absorbance spectra compare well with the corresponding measurements.

1. Introduction

Nanocrystals are fascinating systems spanning sizes from down to around 1 nm up to several hundreds of nanometers forming a rich zoo of different types of nanocrystals, many with very different and unique properties.^[1–4] In particular smaller NCs are of interest as they combine properties of finite sized-system, i.e., molecules with aspects from bulk materials. Controlling the electronic properties of bulk materials and even nanostructures remains difficult and can, depending on the system, be very limited. On the other hand, contrary to solid state materials, chemically tailoring the electronic properties of molecular systems is readily possible, however the discrete energy levels of molecules make electronic applications difficult. Nanocrystals (NC) in the quantum confinement regime bridge this gap

between the band structure of bulk materials and discrete energy level in molecules, combining the best of both worlds. That is, the band structure description remains approximate valid and we gain a new degree of freedom namely the finite NC surface which can be controlled chemically by, e.g., introducing organic ligands for surface functionalization^[5,6] or controlling the energy level alignment by chemical doping,^[7] moreover the quantum confinement itself provides an efficient means to tailor the bandgap.^[2,7,8] Especially quantum confined silicon nanocrystals have attracted significant interest in the past and synthesis, tailoring absorption and luminescence, and device integration have been extensively addressed.^[2,8–13]


Here, while we also include silicon as reference, we focus on tin and in particular on binary Si/Sn nanocrystals which

are promising candidates for direct bandgap semiconducting materials. For various applications such as next-generation solar-cells, light-emitting diodes, and biomedical applications the optoelectronic properties of NCs in the quantum confinement regime are attractive.^[1,8,11,14,15] In particular group IV semiconductors, such as tin (Sn) and silicon (Si), are very important^[3,16] not only due to their electronic properties but also due to their abundance and nontoxicity, where the abundance is important for large-scale production and the nontoxicity a necessary prerequisite for many biomedical applications.^[3,9,12]

Silicon is the most widely used semiconducting material, however its indirect bandgap limits the efficiency of many photovoltaic and optoelectronic applications.^[13,17] While tin has a direct bandgap in its α -phase (α -Sn), it is also a zero gap semiconductor and its vanishing or negative bandgap,^[18] for that matter make optical applications difficult.^[19] Moreover α -Sn is not stable in bulk at room temperature. Recent experiments showed that for ultrasmall Sn nanocrystals at room temperature, contrary to bulk, the α -phase can be stable.^[16,20] For microplasma-synthesized NCs it was found that for diameters below 4 nm not only β -Sn NCs but also α -Sn NCs occur and that for ultrasmall (≈ 1.6 nm) NCs the α -phase is predominant.^[16] Absorbance measurements found a finite bandgap for these ultrasmall α -Sn nanocrystals,^[16] however whether the gap is indeed direct remains an open question which is difficult to answer by experiment alone. Another strategy to obtain an indirect to direct bandgap transition are alloyed $\text{Si}_{1-y}\text{Sn}_y$

Dr. M. Bürkle, Dr. M. Lozac'h, Dr. C. McDonald, Dr. V. Švrček
National Institute of Advanced Industrial Science and Technology (AIST)
Central 2, Umezono 1-1-1, Tsukuba 305-8568, Japan
E-mail: marius.buerkle@aist.go.jp

Dr. M. Macias-Montero, Dr. B. Alessi, Prof. D. Mariotti
Nanotechnology & Integrated Bio-Engineering Centre (NIBEC)
University of Ulster
Ulster, Northern Ireland BT37 0QB, UK

 The ORCID identification number(s) for the author(s) of this article can be found under <https://doi.org/10.1002/adfm.201907210>.

DOI: 10.1002/adfm.201907210

nanocrystals^[21–23] In bulk an indirect to direct bandgap transition occurs in alloyed $\text{Si}_{1-y}\text{Sn}_y$ for $y \approx 0.25$,^[24] recent experiments succeeded by means of laser ablation to synthesize silicon–tin NCs in the quantum confinement regime with diameters between 1 and 5 nm^[21,23] and somewhat larger silicon–tin NCs with diameters of around 15 nm were fabricated in silicon matrices.^[22] Whether and if so, at what concentrations an indirect to direct bandgap transition occurs in alloyed silicon–tin NCs remains an open question.

In this work, we provide a theoretical study complemented by of the aforementioned ultrasmall Sn NCs and alloyed $\text{Si}_{1-y}\text{Sn}_y$ NCs focusing on the possibility of direct bandgaps in NCs and optical properties. The theory efforts are complemented by optical absorbance measurements for selected Si NCs. We validate our theoretical predictions with available experimental evidence, while going beyond the current boundaries of experimental capabilities. In the following the term bandgap has to be used with caution as energy bands are strictly speaking a property of bulk materials that is not valid for finite sized-objects such as NCs. However, for systems such as the NCs discussed here, which are in the intermediate regime between molecules with discrete energy levels and bulk with continuous energy bands, it is possible to obtain an approximate band structure in terms of quasibands that include surface and quantum confinements effects but still allows an intuitive interpretation following the traditional band structure theory.^[7,25] Moreover the quasi-band structure is closely related to angle-resolved photoemission spectroscopy (ARPES) of electronic states, which can be used for molecular systems to image and determine the energy of molecular wavefunctions^[26,27] as well as probing the band structure of bulk and thin-film materials.^[28,29]

Using density functional theory (DFT) based electronic structure we show that in terms of the quasibands ultrasmall Sn NCs have indeed a direct bandgap. Moreover for concentrations of $y \approx 0.4$ alloyed $\text{Si}_{1-y}\text{Sn}_y$ exhibits an indirect to direct bandgap transition. Comparing the bandgaps directly with experiment is however difficult due to the shortcomings of DFT to describe the bandgaps of semiconductors accurately, therefore we calculate for selected NCs many-body GW_0 quasiparticle energies and within the Bethe–Salpeter approach we obtain optical properties which are found to compare well with experimental findings of comparable NCs.

2. Results and Discussion

2.1. Quasi-Band Structure: Direct versus Indirect Bandgap

First, we are going to discuss the formation of bands, or quasibands to be precise, in NCs with increasing particle diameter. With increasing system size the discrete energy levels become more and more dense and band-like structures start to emerge which are additionally broadened, in particular, by finite temperature which leads to the formation of band-like electronic states.^[7] In the following we will not further discriminate between the term quasi-band structure and band structure and stick for simplicity to band structure even though that this is strictly speaking not completely accurate.

The precise shape of the nanoparticles present in experiment is difficult to probe but high-resolution transmission electron microscopy (TEM) suggest the shape to be spherical to a large degree, following our experimental findings,^[10,21] we consider approximately spherical NCs with hydrogen passivation (for details see the Experimental Section). We consider two Si and two α -Sn NCs with diameters of $d = 1.4$ nm and $d = 3.0$ nm for silicon and $d = 1.6$ nm and $d = 3.4$ nm for tin, respectively (inset **Figure 1a–d**). Doubling the particle diameter increases the ratio of the core to surface-atoms from 0.67 for the small NCs to 2.12 for the larger ones. Accordingly, with increasing diameter, i.e., increasing the number of atoms seeing a bulk-like environment, the band-like features in the quasi-band structure become more pronounced (**Figure 1**). For the smaller NCs these features are still washed-out and the discrete levels remain visible, for the larger NCs the features become sharper and valence and conduction bands can be clearly identified, where the high-symmetry points displayed in **Figure 1** are given in terms of the corresponding bulk reciprocal lattice coordinates. Here, it is worth noting that the finite-size effects remain also important for the larger NCs. While clear bands develop, the broken translational invariance of the NCs lattice results that k-points in different Brillouin-zones are not necessarily equivalent. The Si NCs have, similarly to bulk Si, a indirect bandgap with the valence band maximum (VBM) at the Γ_1 -point (Γ_1 -point) and a conduction band minimum (CBM) approximately at X-point. Increasing the NC diameter decreases the degree of quantum confinement and hence the bandgap decreases.^[7] For Sn NCs we observe a direct bandgap at Γ_1 -point (Γ_1 -point). Both the indirect bandgap for Si and the direct bandgap for α -Sn are consistent with what our experimental findings suggest.^[10,16]

2.2. Binary $\text{Si}_{1-y}\text{Sn}_y$ Compound

Next we want to discuss the evolution of the bandgap in alloyed $\text{Si}_{1-y}\text{Sn}_y$ (zinc-blende structure) for the large NC ($d = 3$ nm) with increasing Sn concentration. The alloying is substitutional, that is, silicon atoms in the cubic diamond lattice are replaced by tin atoms. Such substitutional Si/Sn alloys are well known for bulk materials^[24,30] and have been recently observed also for alloyed nanoparticles.^[21–23] The formation of core–shell Si/Sn during ns/fs laser ablation is very unlikely and has not been observed in experiment. In the following we consider low concentrations ($y = 0.12$ and $y = 0.17$), indeterminate ($y = 0.30$), and high concentration ($y = 0.41$) of Sn, where we assume a random fixed distribution of alloy components. The two lowest concentrations of 12% and 17% have been recently experimentally realized in $\text{Si}_{1-y}\text{Sn}_y$ NCs, 30% is the limit for which an indirect to direct bandgap transition has been suggested for bulk $\text{Si}_{1-y}\text{Sn}_y$ alloys, and 41% corresponds to the concentration where the indirect and direct bandgap become comparable in NCs. The corresponding NCs and band structures are summarized in **Figure 1f–h**. For 12% and 17% Sn the bandgap remains clearly indirect and the band structure becomes somewhat more “fuzzy” due to the induced strain,^[7] but remains overall comparable to that of the pristine Si NC with additional bands starting to emerge around the Γ_1 -point (Γ_1 -point). With increasing Sn concentration these additional bands become more and more

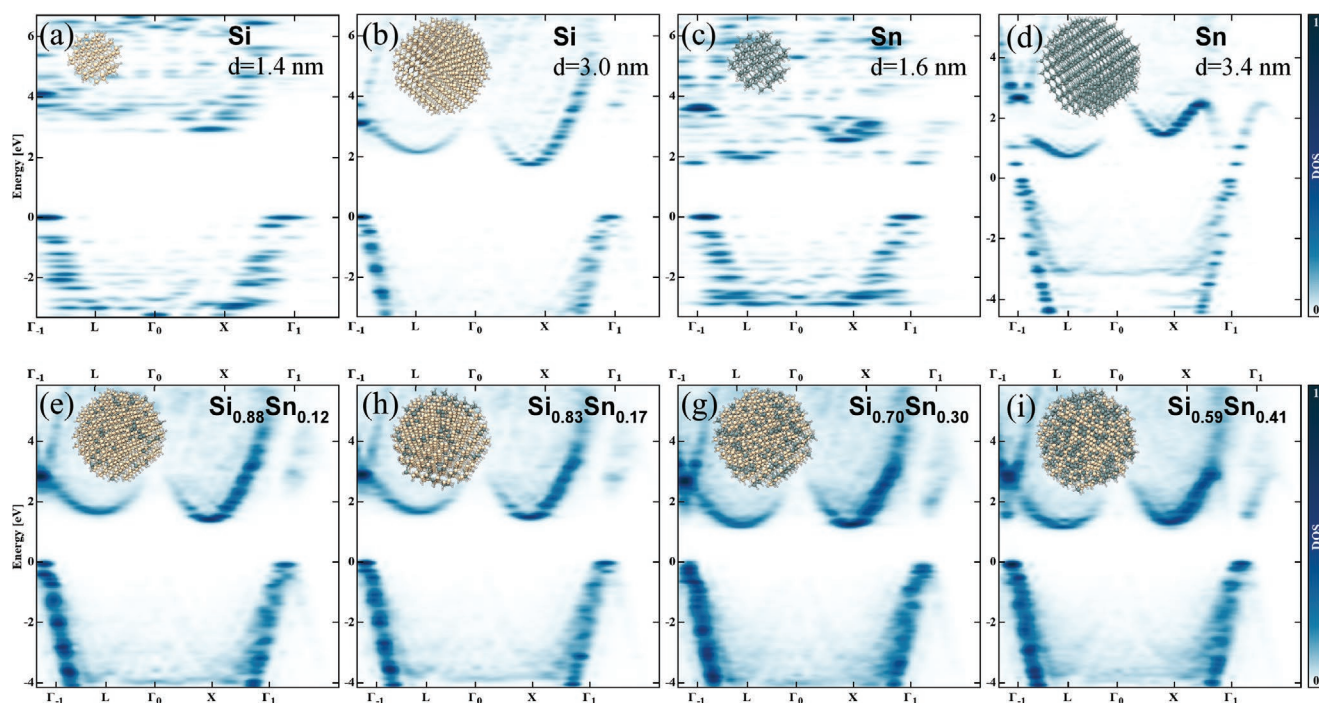


Figure 1. Quasi-band structure for a) Si NC with diameter $d = 1.4$ nm, b) Si NC with $d = 3.0$ nm, c) Sn NC with $d = 1.6$ nm, and d) Sn NC with $d = 3.4$ nm and for $\text{Si}_{1-y}\text{Sn}_y$ NCs with e) $y = 0.12$, f) $y = 0.17$, g) $y = 0.3$, and h) $y = 0.41$. The insets show the corresponding geometrical structure of the NCs.

pronounced and shift toward lower energies, while the rest of the bands remain roughly constant in energy. For the highest concentration of 41% the direct and indirect bandgap are almost comparable with the indirect gap being only slightly smaller than the direct transition (Figure 2). Moreover the CBM is now situated at the L-point and not at the X-point.

To assess the influence of the actual distribution of the binary alloy components, we have calculated for $\text{Si}_{0.7}\text{Sn}_{0.3}$ four

additional structures with a different random distribution of Sn. As summarized in Figure 3 the influence on the band structure is only minor and all the features discussed above remain robust with regard to the actual distribution of the two alloy components. This is also supported by the fact that the overall character of the band structure for increasing random distribution of Sn remains similar and we observe a “continuous” formation of the features due to increasing Sn concentration (Figure 1f–h).

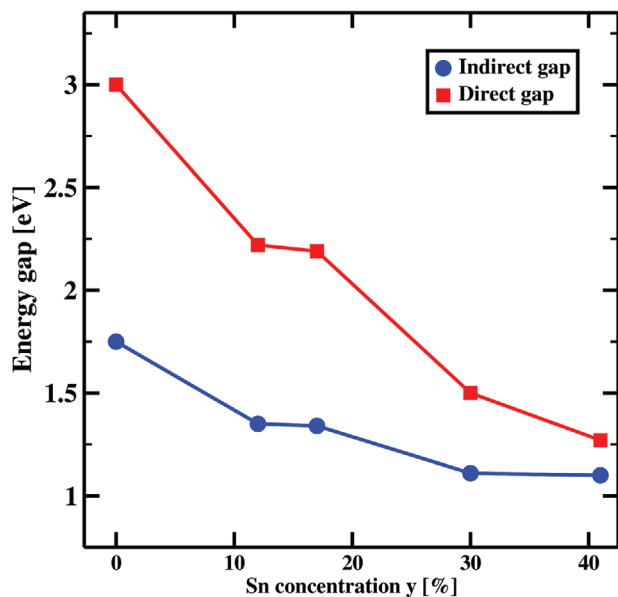


Figure 2. Direct and indirect gaps for different concentrations y of tin in $\text{Si}_{1-y}\text{Sn}_y$.

2.3. Optical Properties

While the quasiband structure derived from DFT gives a good qualitative understanding of the NC's electronic structure, the direct comparison with experiment, in particular for optical gaps usually determined from measured absorbance spectra, is in general not possible. Therefore, we calculated starting from the DFT electronic structure eigenvalue self-consistent GW quasiparticle energies and from the Bethe–Salpeter equation (BSE) the absorbance spectra of the NCs as the imaginary part of the dielectric constant

$$\varepsilon_2(\omega) = \sum_s f_s(\omega) \delta(\omega - \Omega_s) \quad (1)$$

where all prefactors are absorbed in the oscillator strength $f_s = 16\pi^2 e^2 |e \cdot \langle 0 | v | S \rangle|^2 / \Omega_s$ where $e \cdot \langle 0 | v | S \rangle$ is the velocity matrix element along the polarization of the light e for each excited state S with excitation energy Ω_s (for details see the Experimental Section).

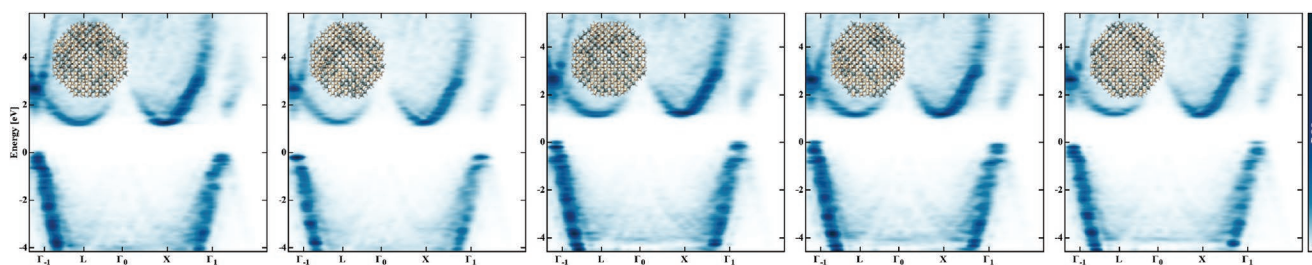


Figure 3. Quasiband structure for $\text{Si}_{0.7}\text{Sn}_{0.3}$ for different distribution of Sn.

The absorption spectra and oscillator strength for each excited state are summarized in **Figure 4**. The lowest lying excitation in the calculated absorbance spectra for the Sn NC particle with $d = 1.6$ nm (Figure 4a) of 2.33 eV compares well to our recent measurements where we obtained an optical gap of 2.2 eV for NCs of comparable size.^[16] From the absorbance spectra of the small NC the discrete levels, suggested from the quasiband structure discussed above, is clearly visible in the absorbance spectra. Accordingly, due to the formation of quasibands for the larger Sn NC ($d = 3.4$ nm) the absorbance spectra (Figure 4b) tends toward bulk spectra,^[31] decreasing the lowest

lying excitation to around 0.98 eV. For silicon we observe a similar behavior, i.e., the discrete levels around the gap for the small NC ($d = 1.4$ nm) gives rise to more distinct features in the absorbance spectra due to individual excitations, (Figure 4c) and the tail at the band edge for energies below 4 eV is due to several excitations with comparably small oscillator strength (inset Figure 4c) which result, however, in a joined band due the finite broadening. Thus giving a well defined optical gap is difficult and it can be expected that the precise surface structure realized experiment may result, depending on experimental conditions, in a varying optical gap. For the larger NCs ($d = 3.0$ nm),

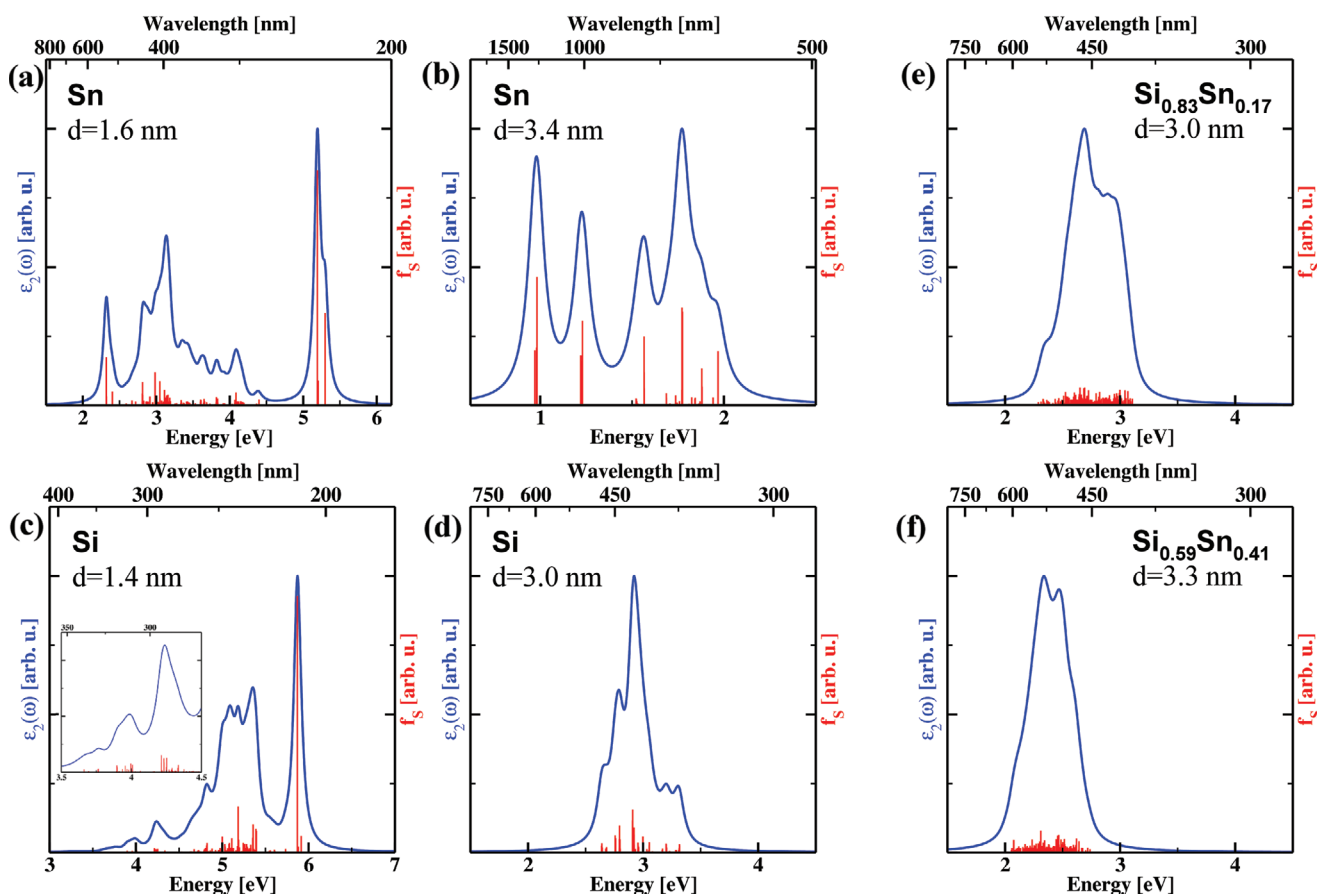


Figure 4. Imaginary part $\epsilon_2(\omega)$ of the dielectric function and oscillator strength f_S for SnNCs with a) $d = 1.6$ nm and b) $d = 3.4$ nm, Si NCs with c) $d = 1.4$ nm and d) $d = 3.0$ nm, and $\text{Si}_{1-y}\text{Sn}_y$ NCs with e) $y = 0.17$ nm and f) $y = 0.41$ nm. A Lorentzian broadening of 0.05 eV is applied to the dielectric function $\epsilon_2(\omega)$. The inset of (c) shows a zoom in to the low energy tail to highlight small but dense f_S not visible in the full plot.

on the other hand, the states become much denser around the gap, accordingly they merge to a single peak (Figure 4d) which give a more well defined optical gap between 2.7 and 3.0 eV.

Next we look at the dependence of the absorbance spectra on the Sn concentration in $\text{Si}_{1-\gamma}\text{Sn}_\gamma$ alloyed NCs which is summarized in Figure 1. As evident from the quasi-band structure (Figure 1f–h) and the distribution of the excited states (Figure 1) alloying the Si NC introduces additional states in the vicinity of the band edges of the CBM and VBM, accordingly the dense quasibands give rise to a single well defined peak in the absorbance spectra. Increasing the Sn concentration narrows the absorbance peak and shifts the energy of the gap and excited states in general down in energy.

3. Conclusion

In summary the quasi-band structure approach allowed us to connect the electronic structure of finite-sized ultrasmall nanocrystals with the intuitive concept of solid state band structure calculations. We have demonstrated that from the discrete electronic states of small nanocrystals in the quantum confinement regime electronic bands can emerge if the system-size is increased. This approximate band structure allowed us to show that α -Sn nanocrystals have a finite and indeed direct bandgap as it was suggested by recent experiments and that the bandgap for Si nanocrystals on the other hand remains indirect. While for ultrasmall nanocrystals the discrete energy levels are still clearly evident in the quasi-band structure, for larger diameter pronounced bands emerge, however finite-size effects remain important. For alloyed silicon/tin nanocrystals we found that the indirect to direct bandgap transition for $\text{Si}_{1-\gamma}\text{Sn}_\gamma$ occurs at higher concentration, namely for $\gamma > 0.41$, than in its bulk counterpart. The optical properties of these nanocrystals were studied by a GW_0 +BSE approach and we showed that the degree to which band-like electronic states are formed is also evident in the absorbance spectra. Lastly, we compared the measured and calculated absorption coefficient for silicon nanocrystals with a diameter of 2.2 nm and found excellent agreement with between measurement and theory.

4. Experimental Section

Computational Method: To model the nanocrystal geometry an initial structure with a certain diameter cutout from a bulk diamond cubic lattice with undercoordinated surface atoms removed was generated. After undercoordinated atoms were removed the NC was composed of faces of (100) and (111) surfaces, which followed what had been reported for the equilibrium structure of silicon.^[32] The NCs were fully passivated by hydrogen. Within DFT, as implemented in the first-principles package Conquest, the resulting structures were fully relaxed until the maximum norm of the residual force dropped below 10^{-4} a.u., whereby the calculations were performed using the Perdew, Burke, and Ernzerhof (PBE) functional^[33,34] using a single- ζ polarization (SZP) basis set derived from norm-conserving pseudopotentials^[35,36] with a grid cutoff of 100 Ha. From the electronic structure of the relaxed geometries the quasi-band structure was obtained by means of Green's functions following ref. [7].

The initial mean-field electronic structure and dipole matrix elements were calculated using the first-principles package Octopus which does not depend on a basis set but uses a grid to directly represent fields in real-space.^[37] Here the same parameters used for the quasi-band

structure calculations were employed, saved for omitting the nonlinear core-corrections present in the pseudopotentials. While the convergence of the DFT self-consistent cycle was somewhat slower without nonlinear core-corrections the impact on the Kohn–Sham eigenvalues was found to be negligible. The initial mean-field electronic structure and dipole matrix elements obtained from Octopus were then used to obtain the optical properties by combining eigenvalue self-consistent evGW quasiparticle calculations^[38–40] with the BSE method as implemented in BerkeleyGW v2.0.^[41] To obtain quasiparticle energies, starting from a G_0W_0 , a evGW calculation was performed where the quasiparticle energies were updated in the noninteracting Green's function while the wavefunctions were kept fixed at their mean-field values.^[42] The quasiparticle energies were converged until their mean-change dropped below 10^{-5} a.u. For the GW calculation the generalized plasmon pole model (PPM) of the dielectric response frequency dependence^[38] with a screening cutoff energy of 9 a.u. and a sum over unoccupied states with energies up to $\approx 15\%$ of the screening cutoff was used. Without the plasmon pole approximation the calculations in this work would be computationally unfeasible. But one should note that the PPM assumes a single charge-neutral excitation and is mainly applied to periodic (crystalline) systems, for finite systems, however, the excitations are not necessarily collective thus the PPM is not rigorously justified here.^[42] However, in practice it has been shown that the generalized PPM calculations perform well also for molecular systems.^[43] Moreover, the systems studied here, while still finite, are tending already toward bulk and are somewhere in between molecules and bulk, thus the applicability of generalized PPM is justified. Subsequently the exciton binding energies and optical absorption spectra were obtained by means of the BSE method,^[41] where the 25 valance highest and 25 lowest conductance bands (states) were included into the BSE kernel.

Supporting Information

Supporting Information is available from the Wiley Online Library or from the author.

Acknowledgements

This work was supported partially by the Japanese Society for the Promotion of Science (JSPS), and by the New Energy and Industrial Technology Development Organization (NEDO).

Conflict of Interest

The authors declare no conflict of interest.

Keywords

absorption measurements, bandgap engineering, direct bandgap nanocrystals, electronic structure calculations, silicon nanocrystals, silicon–tin nanocrystals

Received: September 2, 2019

Revised: February 25, 2020

Published online:

[1] S. K. Nune, P. Gunda, P. K. Thallapally, Y. Y. Lin, M. L. Forrest, C. J. Berkland, *Expert Opin. Drug Delivery* **2009**, 6, 1175.

[2] M. V. Kovalenko, L. Manna, A. Cabot, Z. Hens, D. V. Talapin, C. R. Kagan, V. I. Klimov, A. L. Rogach, P. Reiss, D. J. Milliron,

- P. Guyot-Sionnest, G. Konstantatos, W. J. Parak, T. Hyeon, B. A. Korgel, C. B. Murray, W. Heiss, *ACS Nano* **2015**, 9, 1012.
- [3] P. Reiss, M. Carrière, C. Lincheneau, L. Vaure, S. Tamang, *Chem. Rev.* **2016**, 116, 10731.
- [4] M. A. Boles, M. Engel, D. V. Talapin, *Chem. Rev.* **2016**, 116, 11220.
- [5] N. Anderson, P. E. Chen, A. K. Buckley, J. De Roo, J. S. Owen, *J. Am. Chem. Soc.* **2018**, 140, 7199.
- [6] Z. Huang, Z. Xu, M. Mahboub, Z. Liang, P. Jaimes, P. Xia, K. R. Graham, M. L. Tang, T. Lian, *J. Am. Chem. Soc.* **2019**, 141, 9769.
- [7] M. Bürkle, M. Lozac'h, C. McDonald, D. Mariotti, K. Matsubara, V. Švrček, *Adv. Funct. Mater.* **2017**, 27, 1701898.
- [8] V. Švrček, K. Dohnalova, D. Mariotti, M. T. Trinh, R. Limpens, S. Mitra, T. Gregorkiewicz, K. Matsubara, M. Kondo, *Adv. Funct. Mater.* **2013**, 23, 6051.
- [9] Y. He, C. Fan, S. T. Lee, *Nano Today* **2010**, 5, 282.
- [10] M. Macias-Montero, S. Askari, S. Mitra, C. Rocks, C. Ni, V. Švrček, P. A. Connor, P. Maguire, J. T. S. Irvine, D. Mariotti, *Nanoscale* **2016**, 8, 6623.
- [11] D. Mariotti, V. Švrček, J. W. J. Hamilton, M. Schmidt, M. Kondo, *Adv. Funct. Mater.* **2012**, 22, 954.
- [12] F. Peng, Y. Su, Y. Zhong, C. Fan, S. T. Lee, Y. He, *Acc. Chem. Res.* **2014**, 47, 612.
- [13] K. Sun, S. Shen, Y. Liang, P. E. Burrows, S. S. Mao, D. Wang, *Chem. Rev.* **2014**, 114, 8662.
- [14] J. De Roo, M. Ibáñez, P. Geiregat, G. Nedelcu, W. Walravens, J. Maes, J. C. Martins, I. Van Driessche, M. V. Kovalenko, Z. Hens, *ACS Nano* **2016**, 10, 2071.
- [15] D. Kim, J. Kim, Y. I. Park, N. Lee, T. Hyeon, *ACS Cent. Sci.* **2018**, 4, 324.
- [16] A. U. Haq, S. Askari, A. McLister, S. Rawlinson, J. Davis, S. Chakrabarti, V. Švrček, P. Maguire, P. Papakonstantinou, D. Mariotti, *Nat. Commun.* **2019**, 10, 817.
- [17] H. J. Xiang, B. Huang, E. Kan, S. H. Wei, X. G. Gong, *Phys. Rev. Lett.* **2013**, 110, 118702.
- [18] G. Allan, C. Delerue, *ACS Nano* **2011**, 5, 7318.
- [19] D. Grützmacher, *Group IV Alloys for Advanced Nano- and Optoelectronic Applications*, John Wiley & Sons, Ltd, New York **2016**, pp. 167–179, Ch. 2.5.
- [20] L. Xu, C. Kim, A. K. Shukla, A. Dong, T. M. Mattox, D. J. Milliron, J. Cabana, *Nano Lett.* **2013**, 13, 1800.
- [21] V. Švrček, D. Mariotti, R. A. Blackley, W. Z. Zhou, T. Nagai, K. Matsubara, M. Kondo, *Nanoscale* **2013**, 5, 6725.
- [22] A. Tonkikh, A. Klavsyuk, N. Zakharov, A. Saletsky, P. Werner, *Nano Res.* **2015**, 8, 3905.
- [23] M. Lozac'h, V. Švrček, S. Askari, D. Mariotti, N. Ohashi, T. Koganezawa, T. Miyadera, K. Matsubara, *Mater. Today Energy* **2018**, 7, 87.
- [24] J. Tolle, A. V. G. Chizmeshya, Y. Y. Fang, J. Kouvetakis, V. R. D'Costa, C. W. Hu, J. Menéndez, I. S. T. Tsong, *Appl. Phys. Lett.* **2006**, 89, 231924.
- [25] P. Hapala, K. C. V. Kúsová, I. Pelant, P. Jelínek, *Phys. Rev. B* **2013**, 87, 195420.
- [26] P. Puschnig, A. D. Boese, M. Willenbockel, M. Meyer, D. Lüftner, E. M. Reinisch, T. Ules, G. Koller, S. Soubatch, M. G. Ramsey, F. S. Tautz, *J. Phys. Chem. Lett.* **2017**, 8, 208.
- [27] H. Yang, A. Liang, C. Chen, C. Zhang, N. B. M. Schroeter, Y. Chen, *Nat. Rev. Mater.* **2018**, 3, 341.
- [28] A. X. Gray, C. Papp, S. Ueda, B. Balke, Y. Yamashita, L. Plucinski, J. Minár, J. Braun, E. R. Ylvisaker, C. M. Schneider, W. E. Pickett, H. Ebert, K. Kobayashi, C. S. Fadley, *Nat. Mater.* **2011**, 10, 759.
- [29] I. I. Klimovskikh, M. M. Otrokov, V. Y. Voroshnin, D. Sostina, L. Petaccia, G. Di Santo, S. Thakur, E. V. Chulkov, A. M. Shikin, *ACS Nano* **2017**, 11, 368.
- [30] K. G. Prasad, M. B. Kurup, A. Bhagawat, *Nucl. Instrum. Methods Phys. Res., Sect. B* **1986**, 15, 698.
- [31] L. Via, H. Höchst, M. Cardona, *Phys. Rev. B* **1985**, 31, 958.
- [32] D. J. Eaglesham, A. E. White, L. C. Feldman, N. Moriya, D. C. Jacobson, *Phys. Rev. Lett.* **1993**, 70, 1643.
- [33] J. P. Perdew, K. Burke, M. Ernzerhof, *Phys. Rev. Lett.* **1996**, 77, 3865.
- [34] J. P. Perdew, K. Burke, M. Ernzerhof, *Phys. Rev. Lett.* **1997**, 78, 1396.
- [35] D. R. Hamann, *Phys. Rev. B* **2013**, 88, 085117.
- [36] M. J. van Setten, M. Giantomassi, E. Bousquet, M. J. Verstraete, D. R. Hamann, X. Gonze, G. M. Rignanese, *Comput. Phys. Commun.* **2018**, 226, 39.
- [37] X. Andrade, D. Strubbe, U. De Giovannini, A. H. Larsen, M. J. T. Oliveira, J. Alberdi-Rodriguez, A. Varas, I. Theophilou, N. Helbig, M. J. Verstraete, L. Stella, F. Nogueira, A. Aspuru-Guzik, A. Castro, M. A. L. Marques, A. Rubio, *Phys. Chem. Chem. Phys.* **2015**, 17, 31371.
- [38] M. S. Hybertsen, S. G. Louie, *Phys. Rev. B* **1986**, 34, 5390.
- [39] M. Rohlfing, S. G. Louie, *Phys. Rev. B* **2000**, 62, 4927.
- [40] A. Stan, N. E. Dahlen, R. van Leeuwen, *J. Chem. Phys.* **2009**, 130, 114105.
- [41] J. Deslippe, G. Samsonidze, D. A. Strubbe, M. Jain, M. L. Cohen, S. G. Louie, *Comput. Phys. Commun.* **2012**, 183, 1269.
- [42] D. Golze, M. Dvorak, P. Rinke, *Front. Chem.* **2019**, 7, 377.
- [43] J. Lischner, S. Sharifzadeh, J. Deslippe, J. B. Neaton, S. G. Louie, *Phys. Rev. B* **2014**, 90, 115130.